

## Chapter

## 1

# Magnetic resonance imaging (MRI) methods in Parkinson's disease

Silvia Mangia, Shalom Michaeli, and Paul Tuite

## Introduction

The revolution created by magnetic resonance imaging (MRI) is a result of its ability to utilize the intrinsic differences in the magnetic properties of tissues to provide information about function, structure, and chemistry. This book provides background on a variety of MRI methods and focuses on their application to neurological conditions that manifest with movement disorders. These disorders include neurodegenerative conditions such as Parkinson's disease (PD), Huntington's disease, and ataxia which are characterized by progressive neuronal loss with accompanying neuropathological changes. Meanwhile other movement disorders are not clearly degenerative and tend to have more subtle structural, functional, and neurochemical changes.

The focus of many chapters herein will be on PD, which constitutes the second most common neurodegenerative disease after Alzheimer's disease (AD), and is the principle focus of many clinicians and researchers in the movement disorders field. It is stated that approximately 1% of those over 65 years of age have PD [1]. As a result there is substantial focus on PD research, and the discoveries made in basic neuroscience that relate to pathogenic mechanisms of PD (or AD for that matter) are often relevant for lesser known neurodegenerative parkinsonian conditions such as multiple system atrophy (MSA) or progressive supranuclear palsy (PSP). Along with the progress made in basic science research, MRI developments have been applied to PD and have begun to show promise as a surrogate biomarker in research studies. As well these techniques may be more useful clinically in looking at other parkinsonian conditions such as MSA and PSP. While MRI is presently not able directly to image dopaminergic

neuronal loss that underlies degenerative parkinsonian conditions, it can provide complementary data to those obtained with nuclear tracer imaging. First, this chapter will provide an overview of MRI methods which will be discussed in much greater depth in subsequent chapters, and we will cover nascent techniques that we are employing at the University of Minnesota that may ultimately help provide an imaging biomarker of disease.

## Iron imaging in PD

Initial MRI work in PD began in the mid 1980s as several groups focused on the paramagnetic effects of iron, which is present in increasing quantities in the basal ganglia in PD [2]. This was followed by the frequently referenced work by Gorell *et al.* in 1995 who utilized  $T_2$  and  $T_2^*$  imaging of the substantia nigra (SN) and showed a separation between those with PD and control participants; the change in relaxation time constants was attributed to increased iron in patients with PD [3].  $T_2^*$  imaging is especially sensitive to local magnetic field inhomogeneities induced for example by iron. The focus on iron in PD imaging has remained an important topic and researchers have often utilized  $T_2^*$ , or its reciprocal  $R_2^*$ , in nigral imaging protocols. Visually obvious changes have been observed at 7 tesla (T) in patients with PD as compared to controls (Figure 1.1) [4]. When the term "iron" is employed in PD imaging manuscripts, this typically refers to non-heme iron as opposed to heme iron, and also relates to bound iron that may be present in ferritin or neuromelanin [5]. However, a small pool of free labile iron may actually be a pathogenic culprit as opposed to iron that is safely bound and tucked away. Nonetheless the overall increase in bound iron seen in PD – which is more

## Chapter 1: MRI methods in Parkinson's disease

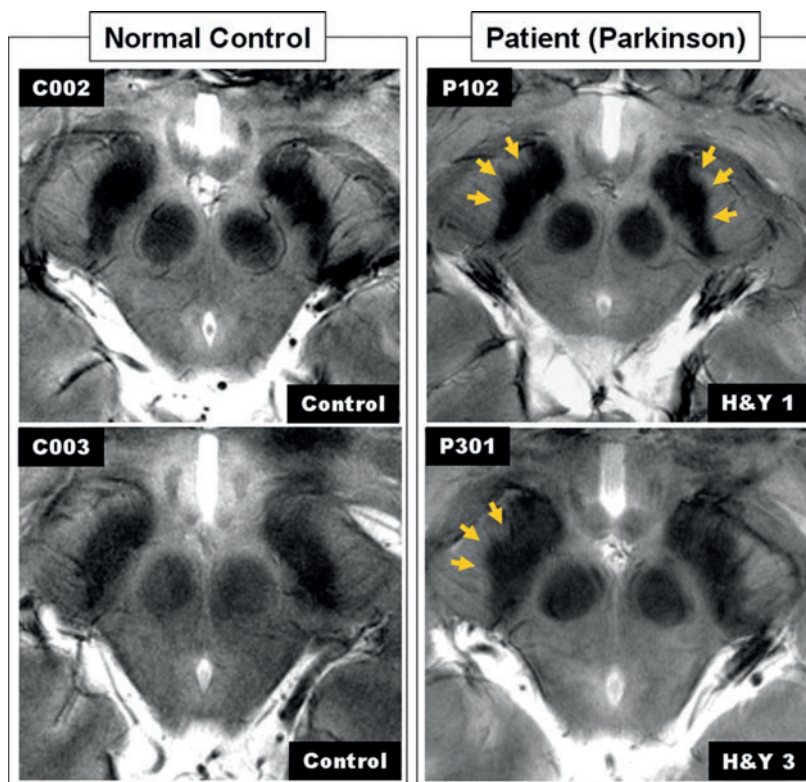


**Figure 1.1** Three-dimensional  $T_2^*$ -weighted gradient echo MRI at 7T of the midbrain. These two PD cases (H&Y 1 and 3 = Hoehn & Yahr stage 1 and 3, respectively) show substantially serrated substantia nigra (SN) in their lateral boundaries compared with normal controls that may represent increased iron accumulation. (Cho *et al.*, 2011 [4].)

than occurs with “normal aging” – may represent a marker of disease and possibly a source for increased free and presumably pathogenic iron [5]. Other important issues to consider about brain iron are the higher concentrations seen in men, as well as the potential for effects from dietary and environmental toxins. Serum ceruloplasmin levels may help address potential confounds in imaging studies [6]. Another factor is the location of iron; whether it is present in neurons or glia such as astrocytes or oligodendrocytes [7]. It is currently not possible to determine whether the imaging abnormalities in PD reflect changes in neuromelanin in dopaminergic neurons or ferritin in glia or neurons. Additionally, while iron changes have been noted in PD, it remains to be determined if iron-sensitive MRI methods will serve as a surrogate of disease – to monitor progression or characterize the severity of disease. This topic will be covered more completely in Chapter 2 by Wayne Martin.

Meanwhile other iron-sensitive methods have been recently developed. These include adiabatic  $T_{2p}$  [8, 9], magnetization transfer (MT) imaging [10–15], and susceptibility-weighted imaging (SWI) [16–20].

## Susceptibility-weighted imaging (SWI)

SWI is a technique that is available on clinical MRI platforms which exploits the differences in magnetic susceptibility between tissues. SWI is based on gradient echo (GRE) pulse sequences with long echo time (TE), and it achieves enhanced image contrast for detecting susceptibility variations from combining magnitude and phase data of the GRE acquisitions. Since iron induces magnetic susceptibility differences, SWI is inherently sensitive to the presence of iron, and is able to demonstrate anatomical structure as well as potentially providing measures of iron content [21]. Much of the recent excitement in movement disorders has arisen from studies conducted at 7T – including work in enhanced visualization of brain surgical targets [16–20], as discussed in Chapter 8.

## Magnetization transfer imaging (MTI)

MTI utilizes the transfer of magnetization between bulk (free) water protons and protons associated with macromolecules [22] and is generally accepted as a correlate of tissue integrity. The detection of the

magnetization transfer (MT) effect in clinical practice is usually limited to the measurement of MT ratios (MTRs), that is, ratios of signal intensity measured with and without the saturation pulse [22]. However, MTRs have appeared to be more useful in atypical parkinsonian conditions than in PD except for one group which showed the potential utility of MTR in PD [10, 12–15]. In contrast to MTR, we have developed an easy-to-implement *quantitative* MT method to estimate MT parameters, which relies on an inversion-prepared MT protocol [11]. By progressively incrementing the duration of the off-resonance continuous wave (CW) pulse, the  $T_1$  of water in the presence of saturation ( $T_{1sat}$ ) and the steady-state (SS) magnetization ( $M_{ss}$ ) can be estimated. In addition, the forward exchange rate from the solid to the free pool,  $k_f$ , can be calculated as  $(1 - M_{ss}/M_0)/T_{1sat}$ . The basic source of instability in the fitting procedure of  $T_{1sat}$  and  $M_{ss}$  originates from the impossibility of using MT pulses that are long enough to achieve the steady state, due to safety limitations imposed by the specific absorption rate (SAR) of radiofrequency (RF) power deposition. To circumvent this limitation, we developed a protocol where two consecutive sets of measurements are acquired with the magnetization initially along the  $-z$  or  $+z$ -axis, that is with or without an on-resonance inversion prior to the off-resonance irradiation. Whereas the usage of inversion recovery approaches has been suggested to measure MT effects [23, 24], the implementation of an on-resonance inversion pulse prior to the off-resonance irradiation has not been exploited so far. We have used the inversion-prepared MT protocol together with adiabatic  $T_{1\rho}$  in a study which aimed at assessing the integrity of the brainstem structures of PD [25]. Results from this study will be discussed in the next section.

## Adiabatic rotating frame relaxation methods

Conventionally, MRI contrast is generated by the tissue variation of free-precession longitudinal (time constant,  $T_1$ ) and/or transverse (time constant,  $T_2$ ) relaxation of the  $^1\text{H}_2\text{O}$  MR signal. These time constants are measured in the laboratory frame, in which the direction of the main magnetic field defines the longitudinal or  $z$ -axis. The free precession relaxation rate constant ( $R_1$ ) is particularly sensitive to magnetic fluctuations that occur as a result of molecular

motion at frequencies near the Larmor precession frequency ( $\omega_0$ ), which falls in the MHz range. However, there is reason also to probe lower frequencies in tissue (i.e., in the kHz range) in order to evaluate for pathology. Rotating frame relaxation rate constants,  $R_{1\rho}$  and  $R_{2\rho}$ , characterize relaxation during radiofrequency (RF) irradiation when the magnetization vector is aligned along or perpendicular to the direction of the effective magnetic field ( $\omega_{eff}$ ), respectively, where the effective magnetic field depends on the applied RF ( $\omega_1$ ) and the frequency offset ( $\Delta\omega$ ).  $R_{1\rho}$  and  $R_{2\rho}$  reflect the features of the spin dynamic processes and depend on the properties of the RF irradiation [26, 27]. Importantly,  $R_{1\rho}$  and  $R_{2\rho}$  are driven principally by dipolar fluctuations at frequencies near the effective precession frequency. Since  $\omega_{eff}$  can be “tuned” by adjustment of the RF amplitude and the frequency offset,  $R_{1\rho}$  and  $R_{2\rho}$  can provide experimental access to the relevant lower frequencies in the range of kHz.

Rotating frame relaxation constants can be measured during the application of adiabatic pulses [28]. In this case, the adiabatic  $R_{1\rho}(t)$  and  $R_{2\rho}(t)$  are time-dependent longitudinal and transverse relaxation rate constants, which characterize decay of magnetization during application of RF pulses operating in the adiabatic regime, that is, when the adiabatic condition (i.e.,  $|\gamma^{-1}d\alpha/dt| \ll B_{eff}$ ), is well satisfied. Here  $\alpha$  is the angle between  $B_{eff}$  and the first rotating frame  $z'$ -axis. The pulses used for the measurements are adiabatic full passage (AFP) of the hyperbolic secant family (HSn) (where  $n = 1, 2, 4, 8, \dots$ ). Detailed descriptions of HSn adiabatic pulse modulation functions are given in Michaeli *et al.* [26, 27]. Briefly, HSn pulses are stretched versions of the hyperbolic secant (HS) pulse [29] and  $n$  denotes the stretching factor. According to this description, the original hyperbolic secant pulse is referred to as the HS1 pulse. As  $n$  becomes larger, the HSn pulse amplitude modulation (AM) function becomes flatter. Thus, the time evolution of magnetization during an HSn pulse can change significantly with a change of  $n$ . During adiabatic pulses the  $R_{1\rho}(t)$  is time dependent as a result of modulating the pulse functions,  $\omega_1(t)$  and  $\omega_{RF}(t)$ . Here,  $\omega_1(t)$  and  $\omega_{RF}(t)$  each have units of radian/s. We have shown that the instantaneous relaxation rate constants during AFP pulse resemble pulse modulation functions and their magnitude depends on the effective frequency  $\omega_{eff}(t)$ . If the magnetization  $M$  is initially not perturbed and the train of the AFP pulses

## Chapter 1: MRI methods in Parkinson's disease

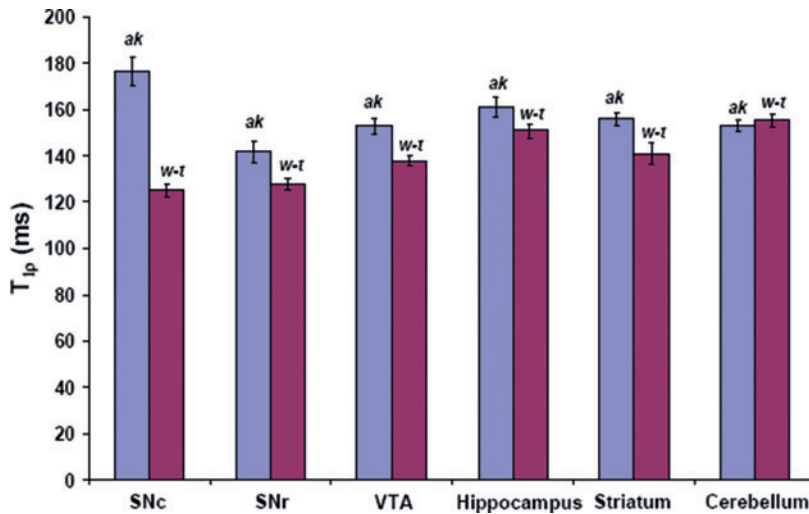


**Figure 1.2**  $T_{1\rho}$  time constants measured in different areas of *aphakia* (**ak**) and wild-type (**w-t**) mice using HS1 AFP pulses. SNc = substantia nigra pars compacta; SNr = substantia nigra reticulata; VTA = ventral tegmental area. (Michaeli *et al.*, 2009 [31].) These findings show that in **ak** mice with absence of SNc neurons there is an increase in  $T_{1\rho}$  as compared to the **w-t** mice in this region.

is applied, the relaxation is governed solely by  $R_{1\rho}$  mechanisms. If magnetization  $M$  is initially excited to  $90^\circ$  and is located in the  $xy$  plane of the laboratory frame and the train of AFP pulses is applied, relaxation is solely  $R_{2\rho}$ . Overall, adiabatic  $R_{1\rho}$  ( $= 1/T_{1\rho}$ ) and  $R_{2\rho}$  ( $= 1/T_{2\rho}$ ) provide novel tissue MRI contrast [26, 27, 30], and allow for determination of fundamental MR parameters, which are rotational correlation times at specific sites,  $\tau_c$ , apparent populations, and exchange relaxation rate constants [31]. The  $R_{1\rho}$  and  $R_{2\rho}$  measured during adiabatic pulses were demonstrated to be sensitive to neural integrity and iron accumulation, respectively [8, 9, 31, 32]. In a validation study of an *aphakia* mouse model,  $T_{1\rho}$  was indeed able to separate *aphakia* versus wild-type mice in the substantia nigra pars compacta (SNc), where there is a congenital absence of dopaminergic neurons (Figure 1.2) [31]. In human studies of PD patients and healthy controls, we have shown the ability of adiabatic methods to detect midbrain changes in PD (Figure 1.3) [8, 9]. Table 1.1 shows the separation of group data using these techniques [8]. Additional recent work has shown that adiabatic methods were able to demonstrate midbrain and medullary changes in PD as compared to controls, as demonstrated in Figure 1.4 [25]. In this figure, the representative  $R_{1\rho}$  and  $R_{1sat}$  maps from control (top) and PD (bottom) subjects are shown. All PD patients were Hoehn and Yahr stage 2, average motor Unified Parkinson Disease Rating Scale (part III) scores were 33.8 (off medication), and average disease duration

was 6 years. Analyses were performed with ten age-matched control subjects. The regions of interest (ROIs) are indicated on the  $T_2$ -weighted images. The differences between the  $R_{1\rho}$  values measured from a rostral region used as internal control per subject (here identified by ROI-1) minus the  $R_{1\rho}$  values measured from medullary nuclei (i.e., ROI-5 and ROI-1 versus ROI-6) were altered in patients relative to control subjects ( $p = 0.004$  and  $p = 0.033$ , respectively). Differences in  $R_{1\rho}$  values were six and eight times larger in patients than in controls when comparing ROI-1 versus ROI-5 and ROI-1 versus ROI-6, respectively. Since  $R_{1\rho}$  values in ROI-1 were not different between patients and controls ( $p = 0.25$ ), these findings represent a change in imaging parameters from areas that contain medullary nuclei that are known to be affected in PD. Interestingly, no statistical differences were observed between patients and controls when considering  $R_{1sat}$ . This could be attributed to differential sensitivity to the exchange regime between  $T_{1\rho}$  and  $T_{1sat}$  [11]. Together, the findings of this study might indicate functional changes that occur prior to neuronal death within the medullary nuclei.

### Relaxations along a fictitious field (RAFF)

A potential limitation to the widespread exploitation of rotating frame relaxation in PD is the required RF power delivered to the sample (i.e., specific

absorption rate – SAR), which can result in tissue heating. However, RF power can sometimes be reduced by using off-resonance irradiation to create the locking field,  $B_{\text{eff}}$  [33, 34]. Recently we have developed a novel rotating frame relaxation

**Table 1.1.** Averaged calculated  $T_{2p}$ ,  $T_{1p}$ , and  $T_2$  time constants in PD patients and controls

Time constants (ms)	$T_{2p}^a$	$T_2^b$	$T_{1p}^c$
Controls	$72.3 \pm 3.4$	$59.4 \pm 4.3$	$156 \pm 6.7$
PD	$64.6 \pm 3.4$	$57.1 \pm 4.2$	$178 \pm 11.6$

<sup>a</sup> Significant difference between PD and controls ( $p < 0.01$ , two-tailed).

<sup>b</sup> No difference between PD and controls ( $p = 0.32$ , two-tailed).

<sup>c</sup> Significant difference between PD and controls ( $p = 0.036$ , two-tailed).

experiment called Relaxation Along a Fictitious Field (RAFF). RAFF does not require an initial rotation of the magnetization to a specific locking angle. As compared to CW  $T_{1p}$  and adiabatic  $T_{1p}$  and  $T_{2p}$  methods, RAFF experiments can be performed with reduced RF power because the spin-locking field (i.e., the so-called fictitious field  $E$ ) is produced by taking advantage of both amplitude and frequency modulation functions (AM *sine* and FM *cosine*, respectively) operating in a sub-adiabatic condition [34]. RAFF comprises  $T_{1p}$  and  $T_{2p}$  mechanisms by exploiting relaxation in a second rotating frame. RAFF was able to provide a greater contrast in tissues of the SN as compared to  $T_{1p}$  and  $T_{2p}$ , and specifically it was better than all other methods in separating the SN into its various subregions, that is, the pars compacta from pars reticulata [35]. Additional studies are warranted to sort out its utility.

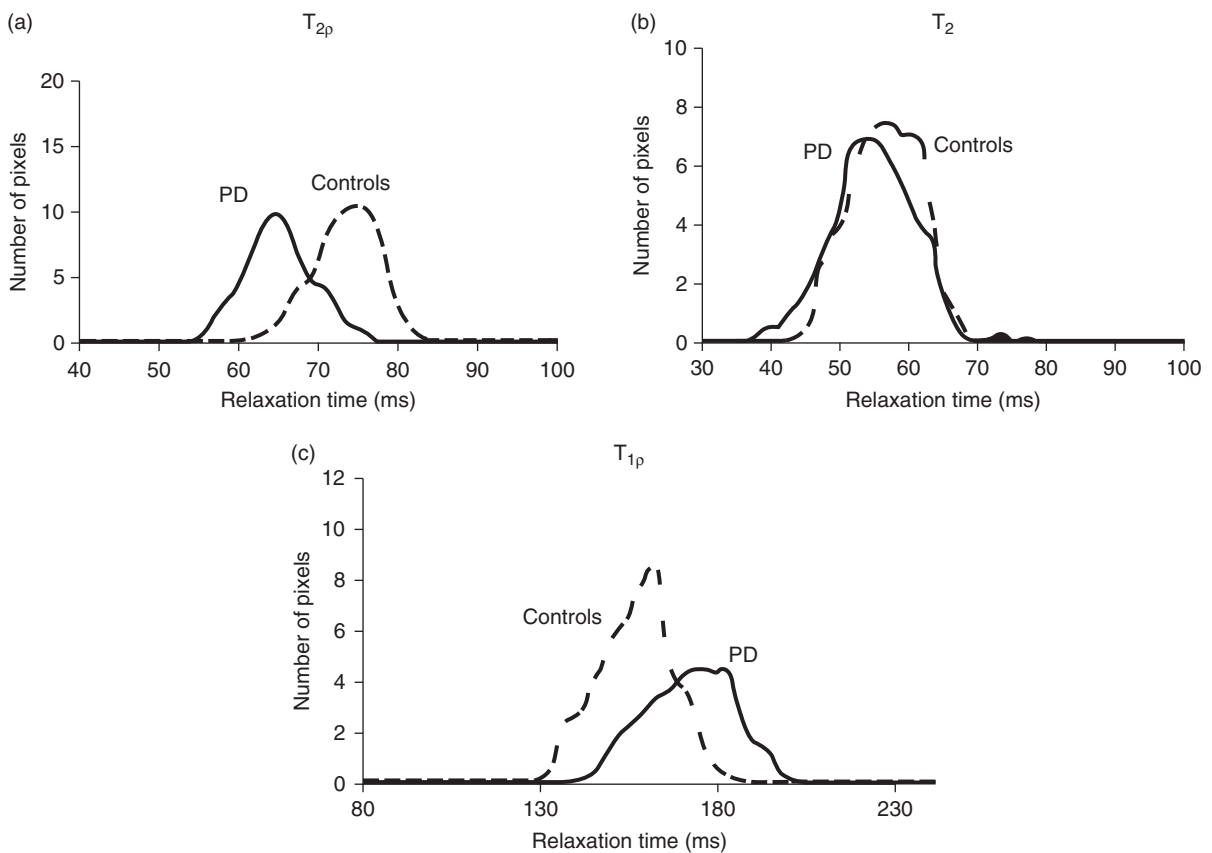


**Figure 1.3** (a) Comparison between  $T_{2p}$  relaxograms in the SN area from PD patients and controls. (b) Comparison between  $T_2$  relaxograms in the SN area from PD patients and controls. (c) Comparison between  $T_{1p}$  relaxograms in the SN between PD patients and controls. ROI obtained from 8 healthy controls and 8 patients with PD. (Michaeli *et al.*, 2007 [8]). ROI, region of interest.

## Chapter 1: MRI methods in Parkinson's disease

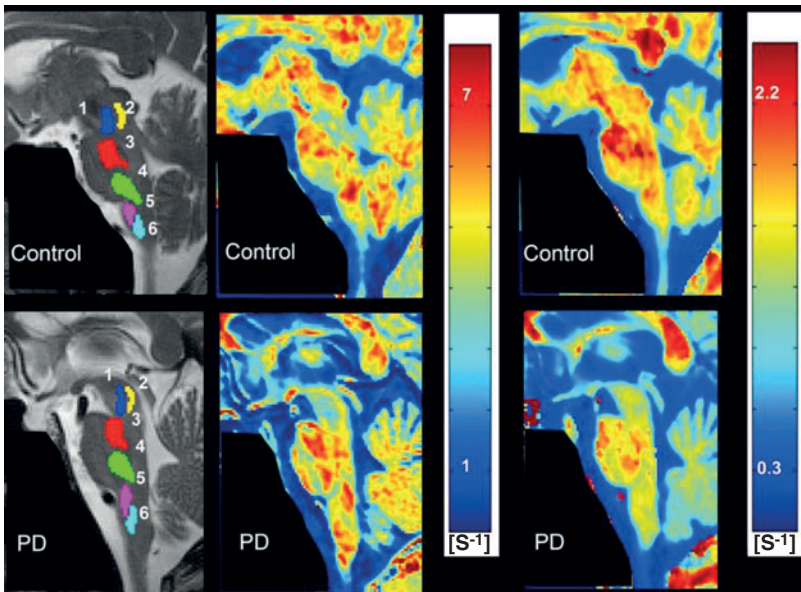


**Figure 1.4** Rotating frame  $R_{1\rho}$  maps (middle column), MT rate maps ( $R_{1sat}$ ) (right column), with relative  $T_2$ -weighted ( $T_2w$ ) images (left column) from representative control subject (top row) and PD patient (bottom row). Regions of interest (ROIs) – as depicted on  $T_2w$  images – were obtained in maps from six areas: (1) medial raphe nucleus; (2) dorsal raphe nucleus; (3) nucleus raphe pontis; (4) nucleus raphe magnus; (5) nucleus raphe pallidus; (6) nucleus raphe obscurus. (Tuite *et al.*, 2012 [25].) See text for details.

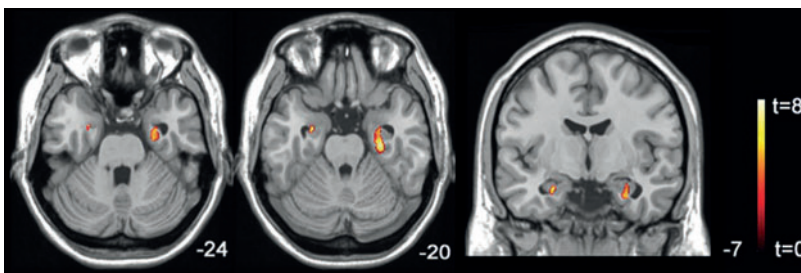


**Figure 1.5** Statistical parametric mapping (t-statistic) axial intensity projection maps rendered onto a stereotactically normalized magnetic resonance imaging (MRI) scan, showing areas of significant increases (colour code, yellow to orange) of gray matter density values in a cohort of patients with idiopathic rapid eye movement sleep behaviour disorder versus healthy control subjects. The number at the bottom right corner of each MRI scan corresponds to the z coordinate in Talairach space. (Scherfler *et al.*, 2011 [39].)

## Volumetric measurements and diffusion tensor imaging (DTI)

Meanwhile researchers have pursued other imaging methods to confirm the known loss of neurons and shrinkage of the SN in PD, with measurements of area or volumes beginning in the early 1990s [36]. These attempts utilized a preselected ROI and subsequently compared affected to unaffected individuals. However, there has been greater refinement with the utilization of methods that do not employ a-priori ROIs. One such method is voxel-based morphometry (VBM), in which there is standardization of data and then voxel-by-voxel comparison between group data to determine if there are differences in signal intensity. VBM discussions will be covered in an assortment of chapters as they relate

to different movement disorders. These methods utilize 1.5 or 3T  $T_1$  anatomical data, which may not be sufficiently sensitive to detect structural changes in PD until there is substantial disease progression and the presence of accompanying dementia [37, 38]. Conditions such as Huntington's disease, MSA, PSP, along with AD and atypical dementias may lend themselves to greater utilization of these methods because atrophy is more prominent and therefore detected earlier. One example of the potential utility of VBM is from a rapid eye movement sleep behavior disorder (RBD) study that showed changes in a population of individuals with RBD as opposed to controls – RBD may represent a precursor to PD in some situations (Figure 1.5) [39]. Meanwhile, researchers are utilizing higher field strengths along with potentially

Cambridge University Press

978-1-107-02636-0 - Magnetic Resonance Imaging in Movement Disorders: A Guide for Clinicians and Scientists

Paul Tuite and Alain Dagher

Excerpt

[More information](#)

## Chapter 1: MRI methods in Parkinson's disease

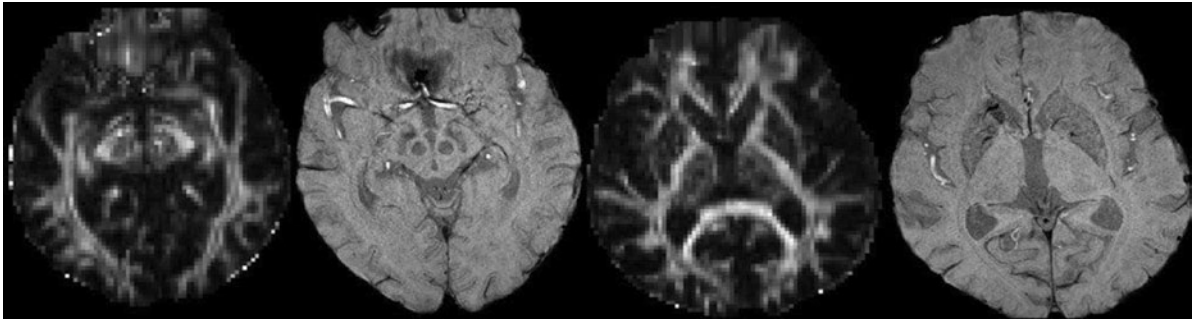


**Figure 1.6** Representative fractional anisotropy (FA) maps from different slices with the corresponding susceptibility weighted imaging (SWI) images in a PD subject demonstrating feasibility of methods on clinical 3T platforms. (Images provided courtesy of P Tuite, K. Lim, and B. Mueller, University of Minnesota, unpublished data.)

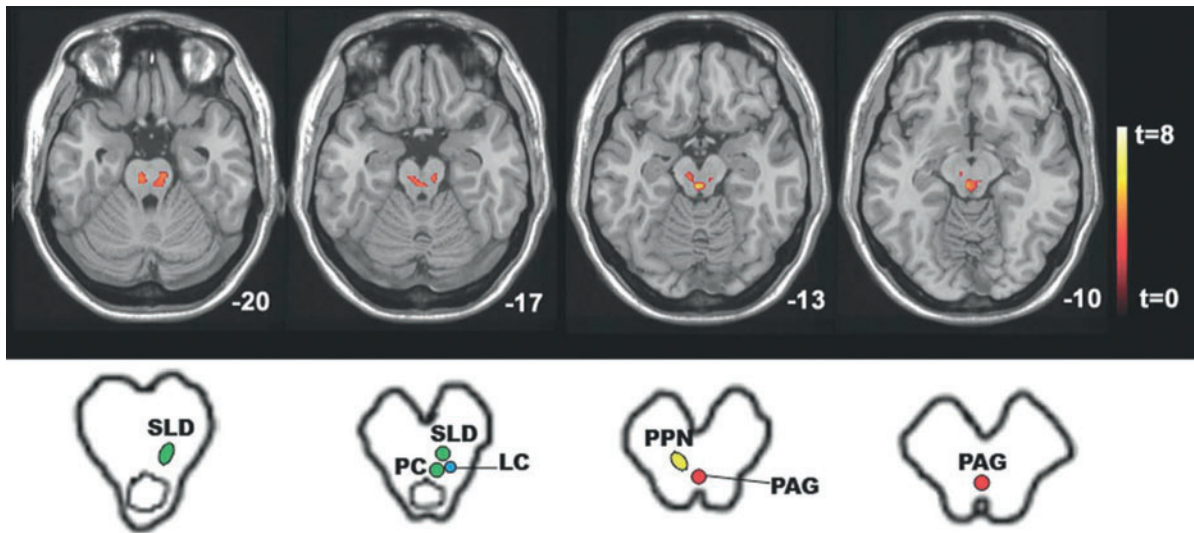


**Figure 1.7** Statistical parametric mapping (t-statistic) axial intensity projection maps rendered onto a stereotactically normalized magnetic resonance imaging (MRI) scan, showing areas of significant increases of mean diffusivity values (colour code, yellow to orange) in a cohort of patients with idiopathic rapid eye movement (REM) sleep behaviour disorder versus healthy control subjects. The number at the bottom right corner of each MRI scan corresponds to the z coordinate in Talairach space. Schematic drawings below correspond to the MRI and visualize proposed nuclei involved in REM sleep control. The REM-off region is represented by the periaqueductal gray matter (PAG) in red, and the REM-on region is represented by the precoeruleus (PC) and sublateralodorsal nucleus (SLD) in green. Nuclei in yellow and blue are known to influence REM and non-REM sleep circuits. LC = locus coeruleus; PPN = pedunculopontine nucleus. (Scherfler *et al.*, 2011 [39].)

more sensitive methods such as  $T_{1\rho}$  or others to generate raw structural data that may provide renewed interest in VBM for PD.

### Diffusion tensor imaging (DTI)

DTI provides structural data based on the directionally restrained diffusion of water within fiber tracts. The movement of water, and hence protons, in white matter tends to be constrained to the long axis of fiber

tracts, leading to anisotropy, that is, greater random motion in certain directions. Pathological processes disturb this natural state of anisotropy and this can be exploited with imaging. Specifically, the loss of restriction of water movement within damaged fiber bundles results in reduced anisotropy, which can be characterized as a reduction in fractional anisotropy or FA. Figure 1.6 (P. Tuite, K. Lim, and B. Mueller, unpublished data) demonstrates FA and SWI imaging of the SN and striatum in PD. Figure 1.7 shows

## Chapter 1: MRI methods in Parkinson's disease

changes in mean diffusivity in a cohort of individuals with RBD, a possible precursor to PD [39]. DTI has its limitations in determining directional and spatial anisotropy; hence some individuals have resorted to methods such as tractography, which include probabilistic and streamline tractography. Several groups have funded but unpublished studies that are evaluating these methods as a means for tracking disease and differentiating parkinsonian conditions from one another as well as appreciating the structural substrates that underlie clinical features. A large-scale effort called the human connectome project ([www.humanconnectomeproject.org](http://www.humanconnectomeproject.org)) is under way to advance DTI methods by generating normative imaging along with neurobehavioral and genomic data. This project applies established and novel methods to evaluate structure and function in the brain. The hope is that these data will allow a reference for disease states such as movement disorders.

## Resting-state MRI

The focus of resting-state MRI is on brain activity that occurs in the absence of externally triggered activity. Even in a “resting state” there are physiological variations in brain activity and accompanying blood flow alterations that manifest as fluctuations in the MRI blood oxygen level-dependent (BOLD) signal. Spontaneous correlations in BOLD signal can be utilized to determine the “functional connectivity” between different regions. There have been a fair number of studies in PD [40–45]. Measurement of this fluctuation can be done using a variety of methods, including the amplitude of low frequency fluctuations or ALFF to assess for an index of resting-state brain activity based on the blood flow variability [44]. Resting-state methods allow the determination of spontaneously occurring brain networks, which may distinguish PD from controls; however, in one study 1/3 of those with PD and 1/5 of controls had unusable data due to motion artifact, which may be partially due to the need to assess subjects when they had been off medications for at least 12 hours [44]. Hence while resting-state functional MRI (fMRI) methods are able to provide a rapid and whole brain view of PD their practicality remains to be determined due to possible need for medication withdrawal for imaging.

## In vivo magnetic resonance spectroscopy (MRS)

MRS has failed to demonstrate great utility in movement disorders until recently. This has been due to the low sensitivity of methods and the low concentrations of metabolites of interest. High-field MRS with its greater sensitivity has overcome some limitations and will be discussed in several chapters, including one by Emir and Öz (Chapter 15) who have demonstrated the ability to measure absolute concentrations of various neurochemicals within the SN and other brainstem regions.

Meanwhile, MRS imaging (MRSI) has begun to measure cerebral metabolic rates of oxygen ( $CMRO_2$ ) and ATP ( $CMR_{ATP}$ ) and to correlate neuroenergetics with specific brain functions.  $CMRO_2$  measurements are achieved using inhaled  $^{17}O_2$  gas which is ultimately incorporated into labeled water ( $H_2^{17}O$ ) in brain tissue, which is detectable by in vivo  $^{17}O$  MRS [46, 47]. This method allows the determination of the role of oxygen metabolism in normal brain function and disease to complement functional MRI studies that utilize the BOLD contrast and are sensitive to cerebral blood flow.

Another important development includes in vivo  $^{31}P$  MRSI which generates measurements of intracellular pH and metabolites of ATP, ADP, and phosphocreatine (PCr), among others [47]. The combination of MRSI and magnetization transfer imaging allows for the measurement of  $CMR_{ATP}$ , and hence oxidative phosphorylation, a measure of cerebral mitochondrial function. This may prove useful in PD and Huntington's disease, in which mitochondrial dysfunction is thought to play a key role.

## Clinical applications

MRI methods are seemingly making their way into the clinic; most rapidly by aiding the neurosurgeon in planning targeting for deep brain stimulation (DBS) surgery (Figure 1.8) [48], also discussed in more detail in Chapter 8. Combining information from different modalities may increase sensitivity to disease states, as shown for example in the combination of structural and iron-sensitive imaging (Figures 1.9, 1.10, and 1.11) [49, 50]. It is hoped that cross-sectional and longitudinal studies that are funded through the M. J. Fox Foundation and the

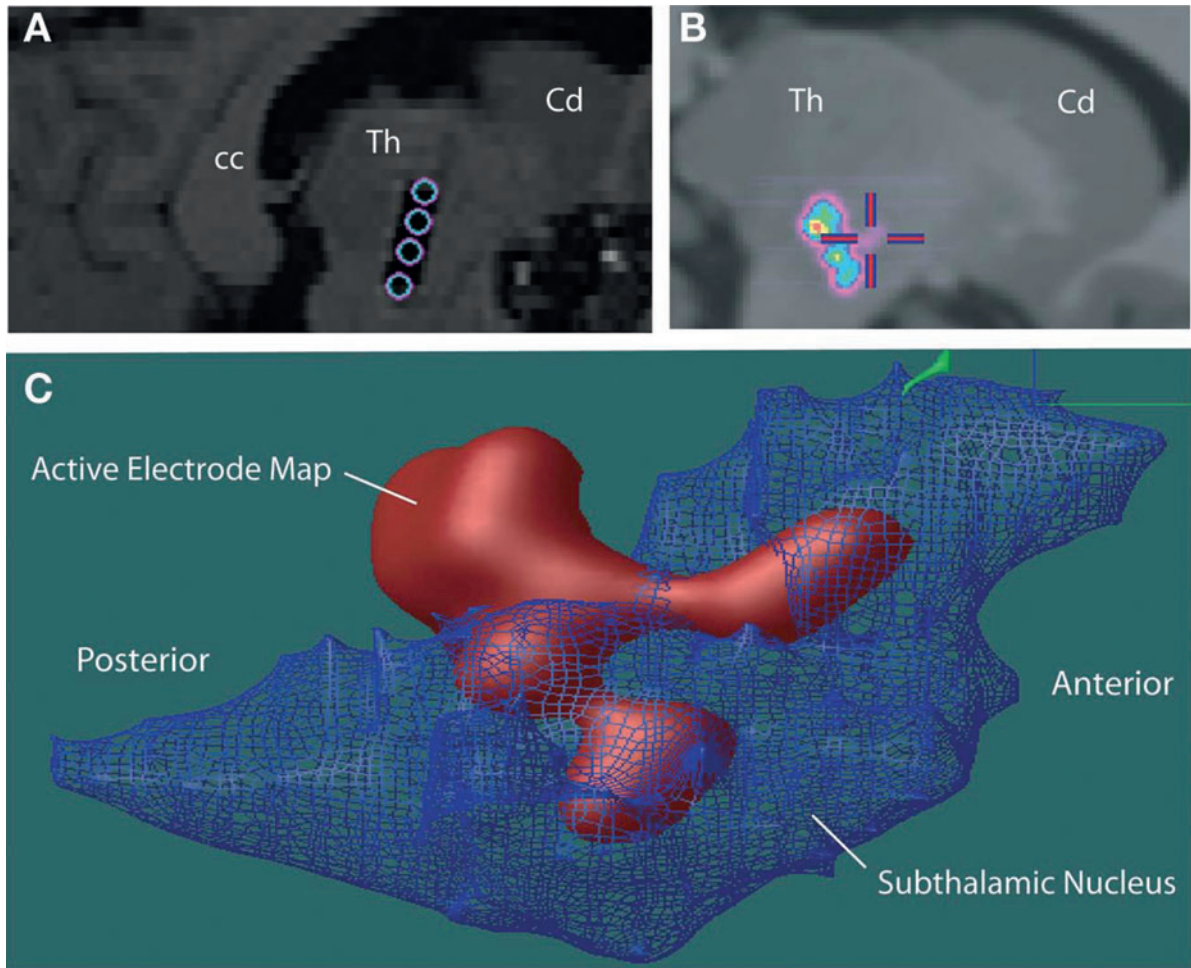


**Figure 1.8** (A) Postoperative sagittal  $T_1$ -weighted MRI scan of a patient who underwent insertion of subthalamic stimulators for Parkinson's disease. The hypointense signal artifact shows the electrode tip (Medtronic 3387) with four contacts indicated by circles that traverse the subthalamic nucleus. The electrode contacts are within, and dorsal to, the subthalamic nucleus. Abbreviations: cc, corpus callosum; Cd, caudate; Th, thalamus. (B) The automatic non-linear image matching and automatic labeling (ANIMAL) algorithm was used to integrate each patient's MRI scan with the canonical high-resolution MRI (Colin27), resulting in a common space for evaluation of electrode positions from different patients. A probabilistic average map of active contacts of subthalamic stimulators associated with the best outcome for motor symptoms of the contralateral side is shown. (C) The voxel-labeled 3D atlas was integrated with the probabilistic volume map of the most effective active electrode contacts in patients with Parkinson's disease with subthalamic stimulator implants. The subthalamic nucleus is represented as a net. A 90% probability map of most effective electrode positions shows they are localized in the dorsolateral subthalamic nucleus, and areas dorsal and posterior to the subthalamic nucleus, including the zona incerta, Forel's fields, and ventral thalamus. (Sadikot *et al.*, 2011 [48].)

National Institutes of Health will provide additional insights for determining the ability of such methods to provide a correlate to disease severity and progression. With a recent dramatic increase in sales of 7T clinical MRI platforms, there has been great haste to use higher-field magnets over the 3T but whether this proves useful as well as feasible for

clinical research studies as well as care of patients will remain to be seen. At our institution 7T pre-operative images already have altered surgical planning; however, whether 7T can improve outcomes has not been proven yet, and researchers will need to be creative to find funding to address this question.

Chapter 1: MRI methods in Parkinson's disease

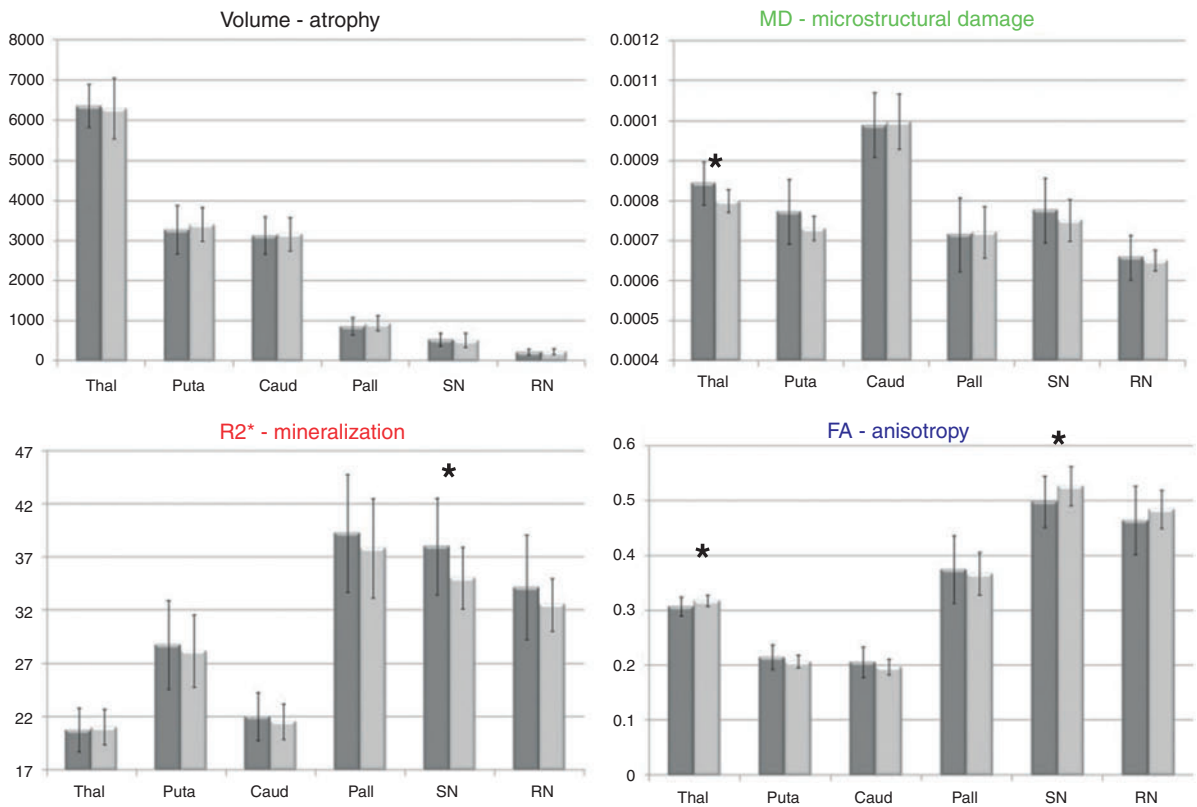
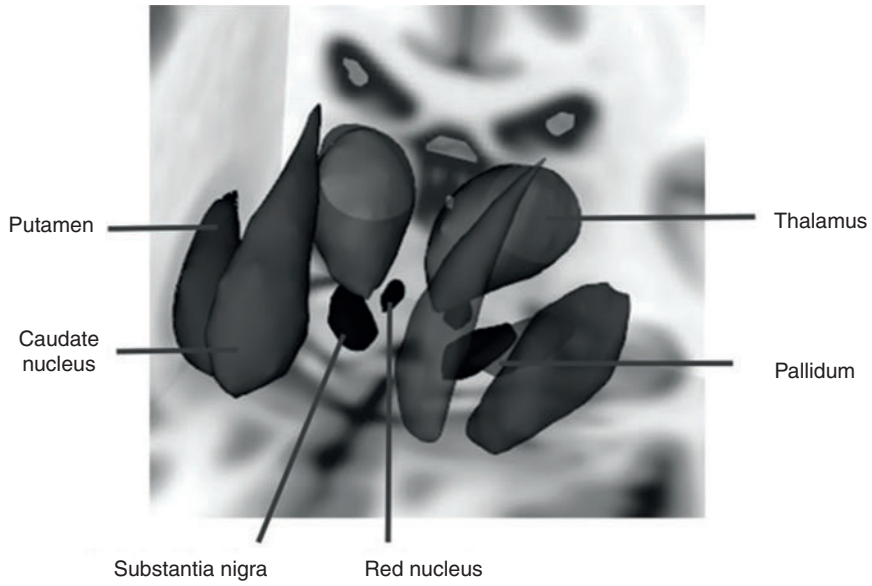


**Figure 1.9** 3D reconstruction of subcortical regions considered in this work (top). Volume (mm<sup>3</sup>), R<sub>2</sub>\* (s<sup>-1</sup>), mean diffusivity (mm<sup>2</sup> s<sup>-1</sup>), and fractional anisotropy mean values from whole subcortical structures (bottom). Light bars = controls, darker bars = Parkinson's disease. \*Significant difference. (Peran *et al.*, 2010 [49].)